CHALMERS
UNIVERSITY OF TECHNOLOGY

Tensioned principle curvature cable nets on minimal surfaces

Tensioned Principle Curvature Cable Nets on Minimal Surfaces

Alexander Sehlström[1,*], Chris J. K. Williams[1],

Department of Architecture and Civil Engineering, Chalmers University of Technology
Gothenburg, Sweden

* Corresponding author e-mail: alexander.sehlstrom@chalmers.se

Abstract

Cable nets are efficient and elegant structures that are pre-stressed to limit their deflection under loading. The best known cable net structure is the Munich Olympia stadium built for the Olympic games in 1972 by Frei Otto and Jörg Schlaich. Frei Otto believed that the ideal shape for such structures is a minimal surface with uniform surface tension under pre-stress. However, a minimal surface can only be approximated by the equal mesh nets used by Frei Otto, but it is possible to produce a true pre-tensioned minimal surface with a fine net of cables forming a pattern of curvilinear squares, which includes a net following the principal curvatures of the surface. Both an analytical and a numerical approach for the form-finding of minimal surfaces with a principal curvature net are described. The analytic approach uses the fact that every minimal surface with principal curvature coordinates can be expressed by a single function of a complex variable. This is a special case of the Weierstrass–Enneper parametrisation which uses two functions, but one of them effectively only controls the pattern of coordinates on the surface. The numerical approach automatically produces a minimal surface and the principal curvature coordinates at the same time and can be applied to any minimal surface whose boundaries are either principal curvature or asymptotic directions, or a combination of the two. Straight lines and cable boundaries form asymptotic lines and a surface which is normal to a sphere has a principal curvature direction as its boundary.

Keywords: cable nets, minimal surfaces, principal curvature, differential geometry, form-finding, conformal mapping

1 Introduction

Cable nets were pioneered by Vladimir Shukhov in the late 19th century with the design of a number of tensile membrane structures serving as exhibition pavilions for the All-Russia Exhibition 1896 in Nizhny Novgorod (Wells 2010). The development accelerated during the 1950s with the completion of the 1953 Dorton Arena in Raleigh, North Carolina by architect Matthew Nowicki and engineer Fred Severud followed by Eero Saarinen and Fred Severud's 1957 Ingalls Ice Rink in New Haven, Connecticut; the French Pavilion at the 1958 Brussels World's Fair by Rene Sarger; the 1958 Sydney Myer Music Bowl by architect Robin Boyd and engineer Bill Irwin (Shaeffer 2013). Further developments were made by Kenzo Tange and Mamoru Kawaguchi with the Yoyogi Arena for the Tokyo Olympics in 1964 (Tsuboi and Kawaguchi 1966), by Frei Otto and Jörg Schlaich with the 1972 Olympic stadium in Munich (Tomlow 2016) and by Hopkins Architects and Expedition Engineering with the 2012 London Olympic Velodrome (Arnold et al. 2011; Wise et al. 2012).

Frei Otto, inspired by Severud's work on the Dorton Arena, devoted his doctoral dissertation 'Das hängende Dach: Gestalt und Struktur' ('The hanging Roof: Shape and Structure') to cable net structures (Otto 1954). Otto believed that the ideal shape for a cable net is a minimal or soap film surface with a uniform surface tension under pre-stress. However it is only possible to approximate a minimal surface with the equal mesh used by Frei Otto. Equal mesh nets, also known as Chebyshev nets (Hazewinkel 1988, p. 123), are easy to lay out out flat on the ground to form a grid of squares before they are raised into position. However it is possible to produce true pre-tensioned minimal surfaces with a net of cables following isothermal coordinates on the surface, that is a pattern of curvilinear squares, subject only to the limitation of the fineness of the grid. It is well known that principal curvature nets on a minimal surfaces can be arranged to form curvilinear squares which edge length is equal to a constant times the square root of the magnitude of the equal and opposite principal radii of curvature. The same applies to asymptotic nets, that is nets in the directions of zero normal curvature which are at 45° to the principal curvature directions on a minimal surface. Cable nets are often pre-stressed with cable boundaries. If the surface is a minimal surface then equilibrium of the cable shows that its curvature in the plane of the surface (the geodesic curvature) is constant, while the curvature normal to the surface is zero. Thus the boundary cable must follow an asymptotic direction on the surface and these asymptotic curves must have constant geodesic curvature.

Even though cable nets have to be designed to carry load, it is usual to find their form assuming no load apart from the pre-stress applied using jacks at the boundaries or under the masts. But before considering such cases, some notes on the geometry of principal curvature nets in general are given in **sec. 2**.

In sec. 3 a pair of surfaces are considered for which the Weierstrass-Enneper parametrisation (Weierstrass 1866) is derived. The parametrisation maps a point on a plane to a point on a minimal surface conformally, that is preserving angles between lines. Two functions of a complex variable are used to define the mapping.

In sec. 4 requirements are imposed so that the coordinates follow the principal curvature directions and then the surface is defined by just one function of a complex variable. The relationship between the Gauss map on an unloaded sphere and a principal coordinate system on a minimal surface is discussed in sec. 5 and the conditions under which unloaded surfaces other than minimal surfaces can be in equilibrium under pretension with the cables following principal curvature directions is examined in sec. 6.

Though analytical approaches may be desirable, there are occasions when numerical form-finding are more suitable and some examples are presented in sec. 7.

Regardless of approach, finding a minimal surface through a given boundary is a variation of Plateau's problem (Douglas 1931; Radó 1933; Harrison and Pugh 2016), but in the case of cable boundaries the boundary shape is determined by the minimal surface itself.

2 Weingarten surfaces

This paper is primarily about unloaded principal curvature nets which are pre-tensioned and in equilibrium under zero applied load. However, it is worth digressing on the geometry of principal curvature nets in general. Throughout the paper, curvilinear coordinates θ^1 and θ^2 will be used for the surfaces, which replace the more usual notation u and v. This enables the use of tensor notation which is useful for geometry, but especially powerful for considering stresses and equilibrium.

The Peterson-Mainardi-Codazzi equations of any surface can be written

$$\nabla_1 b_{\alpha 2} = \nabla_2 b_{\alpha 1}, \tag{1}$$

in which $b_{\alpha\beta}$ are the coefficients of the second fundamental form (Eisenhart (1947) uses $d_{\alpha\beta}$, and Struik (1961) and Rogers and Schief (2002) use e, f, g) and ∇ denotes the covariant derivative (Green and Zerna 1968). Thus for the case $\alpha = 1$,

$$b_{12,1} - b_{\lambda 2}\Gamma^{\lambda}_{11} - b_{1\lambda}\Gamma^{\lambda}_{21} = b_{11,2} - b_{\lambda 1}\Gamma^{\lambda}_{12} - b_{1\lambda}\Gamma^{\lambda}_{21}, \tag{2}$$

where

$$\Gamma^{\lambda}_{\alpha\beta} = \frac{a^{\lambda\mu}}{2}\left(a_{\beta\mu,\alpha} + a_{\mu\alpha,\beta} - a_{\alpha\beta,\mu}\right), \tag{3}$$

are the Christoffel symbols and $a_{\alpha\beta}$ are coefficients of the first fundamental form or the components of the metric tensor (Eisenhart (1947) uses $g_{\alpha\beta}$, and Struik (1961) and Rogers and Schief (2002) use E, F, G). Subscript comma is used to denote partial differentiation.

The conditions for the coordinates on a surface to follow the principal curvature directions are

$$a_{12} = 0, \quad \text{and} \quad b_{12} = 0. \tag{4}$$

Inserting **eq. (4)** into **eq. (2)** yields

$$\left(\frac{b_{11}}{a_{11}}\right)_{,2} = \frac{a_{11,2}}{2a_{11}}\left(-\frac{b_{11}}{a_{11}} + \frac{b_{22}}{a_{22}}\right), \tag{5}$$

and similarly

$$\left(\frac{b_{22}}{a_{22}}\right)_{,1} = \frac{a_{22,1}}{2a_{22}}\left(\frac{b_{11}}{a_{11}} - \frac{b_{22}}{a_{22}}\right), \tag{6}$$

for the case $\alpha = 2$.

The quotients

$$\kappa_{\mathrm{I}} = \frac{b_{11}}{a_{11}}, \quad \text{and} \quad \kappa_{\mathrm{II}} = \frac{b_{22}}{a_{22}}, \tag{7}$$

are the principal curvatures on the surface. Writing

$$a_{11} = E, \quad \text{and} \quad a_{22} = G, \tag{8}$$

we obtain

$$\begin{aligned} \frac{\partial \kappa_{\mathrm{I}}}{\partial \theta^2} &= \frac{1}{2E}\frac{\partial E}{\partial \theta^2}\left(\kappa_{\mathrm{II}} - \kappa_{\mathrm{I}}\right), \\ \frac{\partial \kappa_{\mathrm{II}}}{\partial \theta^1} &= \frac{1}{2G}\frac{\partial G}{\partial \theta^1}\left(\kappa_{\mathrm{I}} - \kappa_{\mathrm{II}}\right), \end{aligned} \tag{9}$$

which are equations (3-8) in Struik (1961), if one replaces θ^1 and θ^2 by u and v.

Let us now introduce the mean curvature, H, the Gaussian curvature, K, and the radius of the Mohr's circle of curvature (Nutbourne 1986), R,

$$\begin{aligned} H &= \frac{\kappa_{\mathrm{I}} + \kappa_{\mathrm{II}}}{2}, \\ R &= \frac{\kappa_{\mathrm{I}} - \kappa_{\mathrm{II}}}{2} = \sqrt{H^2 - K}, \\ K &= \kappa_{\mathrm{I}}\kappa_{\mathrm{II}}, \end{aligned} \tag{10}$$

so that

$$\begin{aligned}\frac{(R+H)_{,2}}{R} &= -\frac{E_{,2}}{E},\\ \frac{(R-H)_{,1}}{R} &= -\frac{G_{,1}}{G}.\end{aligned} \tag{11}$$

The quantities $\sqrt{E}\delta\theta^1$ and $\sqrt{G}\delta\theta^2$ are the spacing between the coordinate curves on the surface. Thus **eq. (11)** control the pattern of lines of principal curvature on a surface.

A *Weingarten surface* (Krivoshapko and Ivanov 2015) is a surface for which there is a functional relationship between the principal curvatures, which can be written as

$$\begin{aligned}H &= H(R),\\ h &= \frac{dH}{dR}.\end{aligned} \tag{12}$$

Weingarten surfaces include minimal surfaces, surfaces parallel to a minimal surface, constant mean curvature surfaces, constant Gaussian curvature surfaces, surfaces of revolution and many others. Integration gives

$$\begin{aligned}\log E &= -\int \frac{1+h}{R}\,dR - P\left(\theta^1\right),\\ \log G &= -\int \frac{1-h}{R}\,dR - Q\left(\theta^2\right).\end{aligned} \tag{13}$$

Setting the arbitrary functions P and Q to zero,

$$\log\left(\frac{E}{G}\right) = \int \frac{2h}{R}\,dR = 2\int \frac{1}{R}\,dH, \tag{14}$$

and

$$EGR^2 = \text{constant}. \tag{15}$$

These two equations gives a unique pattern of principal curvature lines on a surface.

3 Complex pair of surfaces

Consider a pair of surfaces given by the position vectors

$$\mathbf{p}\left(\theta^1,\theta^2\right) = p_x\left(\theta^1,\theta^2\right)\hat{\mathbf{i}} + p_y\left(\theta^1,\theta^2\right)\hat{\mathbf{j}} + p_z\left(\theta^1,\theta^2\right)\hat{\mathbf{k}}, \tag{16}$$

and

$$\mathbf{q}\left(\theta^1,\theta^2\right) = q_x\left(\theta^1,\theta^2\right)\hat{\mathbf{i}} + q_y\left(\theta^1,\theta^2\right)\hat{\mathbf{j}} + q_z\left(\theta^1,\theta^2\right)\hat{\mathbf{k}}, \tag{17}$$

in which $\hat{\mathbf{i}}$,$\hat{\mathbf{j}}$ and $\hat{\mathbf{k}}$ are unit base vectors in the direction of the Cartesian axes x, y and z (Green and Zerna 1968, p. 18).

Now let us stipulate that these Cartesian coordinates are the real and imaginary parts of the complex analytic functions r_x, r_y and r_z of the complex variable

$$\zeta = \theta^1 + i\theta^2, \tag{18}$$

where $i = \sqrt{-1}$ is the imaginary number, so that

$$\begin{aligned} r_x(\zeta) &= p_x(\zeta) + iq_x(\zeta), \\ r_y(\zeta) &= p_y(\zeta) + iq_y(\zeta), \\ \text{and} \quad r_z(\zeta) &= p_z(\zeta) + iq_z(\zeta), \end{aligned} \tag{19}$$

or

$$\mathbf{r}(\zeta) = \mathbf{p}(\zeta) + i\mathbf{q}(\zeta). \tag{20}$$

Note that the Cartesian components remain complex analytic functions if the axes are rotated.

Equation (20) imposes some restrictions on the shape of the surfaces $\mathbf{p}$ and $\mathbf{q}$, but we shall see that *we require further restrictions if we want* $\mathbf{p}$ *and* $\mathbf{q}$ *to be minimal surfaces*.

The complex derivative,

$$\begin{aligned} \frac{d\mathbf{r}}{d\zeta} &= \frac{\partial \mathbf{r}}{\partial \theta^1} = \frac{\partial \mathbf{p}}{\partial \theta^1} + i\frac{\partial \mathbf{q}}{\partial \theta^1} = \mathbf{p}_{,1} + i\mathbf{q}_{,1} \\ &= \frac{\partial \mathbf{r}}{\partial (i\theta^2)} = -i\frac{\partial \mathbf{r}}{\partial \theta^2} = -i\frac{\partial \mathbf{p}}{\partial \theta^2} + \frac{\partial \mathbf{q}}{\partial \theta^2} = \mathbf{q}_{,2} - i\mathbf{p}_{,2}. \end{aligned} \tag{21}$$

Hence

$$\mathbf{p}_{,1} = \mathbf{q}_{,2}, \tag{22}$$

$$\text{and} \quad \mathbf{p}_{,2} = -\mathbf{q}_{,1}, \tag{23}$$

which are the Cauchy-Riemann equations (Spiegel 1974, p. 63) so the map $\mathbf{r}(\zeta)$ is conformal (angle preserving). Therefore, because $\mathbf{p}_{,12} = \mathbf{p}_{,21}$ and $\mathbf{q}_{,12} = \mathbf{q}_{,21}$, the surfaces $\mathbf{p}$ and $\mathbf{q}$ obey the Laplace's equation (Spiegel 1974, p. 63),

$$\mathbf{p}_{,11} + \mathbf{p}_{,22} = 0, \tag{24}$$

$$\text{and} \quad \mathbf{q}_{,11} + \mathbf{q}_{,22} = 0. \tag{25}$$

The surfaces $\mathbf{p}$ and $\mathbf{q}$ share the same tangent plane and unit normal and from **eq. (24)** and **(25)** it can be seen that if unloaded fine grid cable nets were to be constructed from $\mathbf{p}$ and $\mathbf{q}$ in which the *force density* or *tension coefficient* is constant, then the cable nets will automatically be in static equilibrium. The force density is the tension in an element divided by its length (Schek 1974) and therefore if τ is the constant force density corresponding to constant coordinate increments $\delta\theta^1 = \delta\theta^2$, the forces T_i in the four members $i = 1, 2, 3, 4$ meeting at a node are

$$\begin{aligned} T_1 &= -\tau \mathbf{p}_{,1}, \qquad & T_2 &= \tau \left(\mathbf{p}_{,1} + \mathbf{p}_{,11} \delta\theta^1 \right), \\ T_3 &= -\tau \mathbf{p}_{,2}, \qquad & T_4 &= \tau \left(\mathbf{p}_{,2} + \mathbf{p}_{,22} \delta\theta^2 \right), \end{aligned}$$

and so adding and setting the resultant to zero gives **eq. (24)**.

What is more, the surface $\mathbf{q}$ is the three dimensional Cremona-Maxwell diagram (Rippmann 2016; Williams 1986) of $\mathbf{p}$ and vice versa.

At this point, the grid of cables or coordinate curves will not cross at right angles, nor will the cable lengths in the two directions be equal. For this to happen, we need to further stipulate that the scalar product

$$\frac{d\mathbf{r}}{d\zeta} \cdot \frac{d\mathbf{r}}{d\zeta} = 0, \tag{26}$$

which is two equations since both the real and imaginary parts are equal to zero, giving

$$\begin{aligned} \mathbf{p}_{,1} \cdot \mathbf{p}_{,1} - \mathbf{p}_{,2} \cdot \mathbf{p}_{,2} - 2i\mathbf{p}_{,1} \cdot \mathbf{p}_{,2} = \\ -\mathbf{q}_{,1} \cdot \mathbf{q}_{,1} + \mathbf{q}_{,2} \cdot \mathbf{q}_{,2} + 2i\mathbf{q}_{,1} \cdot \mathbf{q}_{,2} = 0, \end{aligned} \tag{27}$$

from which it follows that $E = G$ in **eq. (8)** and

$$\begin{aligned} \mathbf{p}_{,1} \cdot \mathbf{p}_{,1} = \mathbf{p}_{,2} \cdot \mathbf{p}_{,2} = \mathbf{q}_{,1} \cdot \mathbf{q}_{,1} = \mathbf{q}_{,2} \cdot \mathbf{q}_{,2} = L^2, \\ \mathbf{p}_{,1} \cdot \mathbf{p}_{,2} = \mathbf{q}_{,1} \cdot \mathbf{q}_{,2} = 0. \end{aligned} \tag{28}$$

Thus θ^1 and θ^2 form *isothermal coordinate systems* on the two surfaces in which the coordinate curves form curvilinear squares (Struik 1961, p. 171) with side length $L\delta\theta^\alpha$ where $\delta\theta^1 = \delta\theta^2$ is the small increment in coordinates between the curves. The size of the curvilinear squares vary from point to point on the surface.

Equations (24), **(25)** and **(28)** show that the mean curvature of both $\mathbf{p}$ and $\mathbf{q}$ are everywhere zero and they are therefore both minimal surfaces, known as a pair of adjoin minimal surfaces (Struik 1961; Dierkes et al. 2010). We can obtain a

further pair, $\mathbf{P}$ and $\mathbf{Q}$, of adjoin minimal surfaces by writing

$$\mathbf{P} + i\mathbf{Q} = e^{i\varphi}\left(\mathbf{p} + i\mathbf{q}\right), \tag{29}$$

where φ is a real angle representing a rotation of the base vectors around the surface normal. Varying φ does not cause lengths on $\mathbf{P}$ and $\mathbf{Q}$ to change and the deformation of the surfaces is therefore a pure bending with no stretching. $\mathbf{P}$ and $\mathbf{Q}$ are known as associate minimal surfaces of $\mathbf{p}$ and $\mathbf{q}$.

The coordinate curves will in general not follow the principal curvature directions on the surface. For the coordinates to do so, we will need to change coordinates such that the new coordinates, $\theta^{1'} + i\theta^{2'}$ are the appropriate complex function of $\theta^1 + i\theta^1$. We shall return to this in **sec. 4**, but for now, we assume that the coordinates do not follow the principal curvature directions.

If we write

$$\frac{d\mathbf{r}}{d\zeta} = \frac{f}{2}\left(1 - g^2\right)\hat{\mathbf{i}} + i\frac{f}{2}\left(1 - g^2\right)\hat{\mathbf{j}} + fg\hat{\mathbf{k}}, \tag{30}$$

then **eq. (26)** is automatically satisfied. There is nothing unique about this form; any three functions of two independent functions $f(\zeta)$ and $g(\zeta)$ would do provided that the sum of their squares is zero. Then

$$\mathbf{p} = \Re\left\{\int \frac{d\mathbf{r}}{d\zeta} d\zeta\right\}, \tag{31}$$

$$\text{and} \quad \mathbf{q} = \Im\left\{\int \frac{d\mathbf{r}}{d\zeta} d\zeta\right\}, \tag{32}$$

where $\Re\{\}$ and $\Im\{\}$ mean the real respectively the imaginary parts.

Equations (30) and **(31)** are the Weierstrass–Enneper parametrisation of a minimal surface (Eisenhart 1947; Weierstrass 1866) and it can be shown that all minimal surfaces can be expressed in this way.

For any given functions $f(\zeta)$ and $g(\zeta)$, a new function $F(g)$ can always be introduced such that

$$f = \frac{d^3F}{dg^3}\frac{dg}{d\zeta}, \tag{33}$$

and then **eq. (30)** becomes

$$\frac{d\mathbf{r}}{d\zeta}\frac{d\zeta}{dg} = \left(\frac{1}{2}\left(1 - g^2\right)\hat{\mathbf{i}} + i\frac{1}{2}\left(1 + g^2\right)\hat{\mathbf{j}} + g\hat{\mathbf{k}}\right)\frac{d^3F}{dg^3}, \tag{34}$$

which can be integrated by parts three times to give

$$\begin{aligned}\mathbf{r} = &\left(\frac{1}{2}\left(1-g^2\right)\hat{\mathbf{i}}+i\frac{1}{2}\left(1+g^2\right)\hat{\mathbf{j}}+g\hat{\mathbf{k}}\right)\frac{d^2F}{dg^2}\\ &-\left(-g\hat{\mathbf{i}}+ig\hat{\mathbf{j}}+\hat{\mathbf{k}}\right)\frac{dF}{dg}+\left(-\hat{\mathbf{i}}+i\hat{\mathbf{j}}\right)F,\end{aligned} \tag{35}$$

which are the formulae of Weierstrass, (see Struik 1961), and formulae (26) and (28) of section 3.3 'Representations Formulas for Minimal Surfaces', page 117 in Dierkes et al. (2010).

4 Principal curvature coordinates

No assumptions has so far been made about the orientation of the isothermal coordinate system on the minimal surface. It is now time to align the coordinate system with the principal curvature directions.

First, let

$$h(\zeta) = fg, \tag{36}$$

$$\text{and} \quad w(\zeta) = u+iv = \log g, \tag{37}$$

where u and v are real. Substituting into eq. (30),

$$\begin{aligned}\frac{d\mathbf{r}}{d\zeta} &= h\left(\sinh w\,\hat{\mathbf{i}}-i\cosh w\,\hat{\mathbf{j}}-\hat{\mathbf{k}}\right)\\ &= h\left(\left(\sinh u\cos v+i\cosh u\sin v\right)\hat{\mathbf{i}}+\left(\sinh u\sin v-i\cosh u\cos v\right)\hat{\mathbf{j}}-\hat{\mathbf{k}}\right),\end{aligned} \tag{38}$$

which again satisfies eq. (21). The unit normal to the surfaces $\mathbf{p}$ and $\mathbf{q}$ is now simply

$$\mathbf{n} = \frac{1}{\cosh u}\left(\cos v\,\hat{\mathbf{i}}+\sin v\,\hat{\mathbf{j}}+\sinh u\,\hat{\mathbf{k}}\right), \tag{39}$$

which satisfies

$$\mathbf{n}\cdot\mathbf{n} = 1, \tag{40}$$

$$\text{and} \quad \mathbf{n}\cdot\frac{d\mathbf{r}}{d\zeta} = 0. \tag{41}$$

Then

$$\begin{aligned}\frac{d^2\mathbf{r}}{d\zeta^2} &= \mathbf{p}_{,11}-i\mathbf{p}_{,12} = \mathbf{q}_{,12}+i\mathbf{q}_{,11} = -\mathbf{p}_{,22}-i\mathbf{p}_{,12} = \mathbf{q}_{,12}-i\mathbf{q}_{,22} =\\ &= \frac{1}{h}\frac{dh}{d\zeta}\frac{d\mathbf{r}}{d\zeta}+h\frac{dw}{d\zeta}\left(\cosh w\,\hat{\mathbf{i}}-i\sinh w\,\hat{\mathbf{j}}\right),\end{aligned} \tag{42}$$

and

$$\begin{aligned}\mathbf{n}\cdot\frac{d^2\mathbf{r}}{d\zeta^2} &= -h\frac{dw}{d\zeta}\mathbf{n}\cdot(\cosh w\,\hat{\mathbf{i}}-i\sinh w\,\hat{\mathbf{j}})\\ &= -h\frac{dw}{d\zeta}\frac{\left(\cos v\,\hat{\mathbf{i}}+\sin v\,\hat{\mathbf{j}}+\sinh u\,\hat{\mathbf{k}}\right)}{\cosh u}\\ &\quad\cdot(\cosh u\,(\cos v\,\hat{\mathbf{i}}+\sin v\,\hat{\mathbf{j}})+i\sinh u\,(\sin v\,\hat{\mathbf{i}}-\cos v\,\hat{\mathbf{j}}))\\ &= -h\frac{dw}{d\zeta}.\end{aligned} \tag{43}$$

Thus if

$$\Im\left\{h\frac{dw}{d\zeta}\right\}=0 \tag{44}$$

then

$$\mathbf{p}_{,12}=0,\quad \mathbf{q}_{,11}=0,\quad \mathbf{q}_{,22}=0, \tag{45}$$

so then there are principal curvature coordinates on $\mathbf{p}$ and asymptotic coordinates on $\mathbf{q}$, that is coordinates in the directions of zero normal curvature.

Equation (44) is the Hopf holomorphic quadratic differential and is equivalent to equation (30') and Preposition 5 in section 3.1 'Associate Minimal Surfaces', page 99 in Dierkes et al. (2010).

If **eq. (44)** holds, then the Cauchy-Riemann equations give

$$h\frac{dw}{d\zeta}=\Re\left\{h\frac{dw}{d\zeta}\right\}=c=\text{constant}. \tag{46}$$

therefore

$$\mathbf{r}=\mathbf{p}+i\mathbf{q}=\int\frac{c}{\left(\frac{dw}{d\zeta}\right)}\left(\sinh w\,\hat{\mathbf{i}}-i\cosh w\,\hat{\mathbf{j}}-\hat{\mathbf{k}}\right)d\zeta. \tag{47}$$

Unfortunately it is not possible to specify both **eq. (33)** and **(46)** at the same time so one cannot avoid the integration in **eq. (47)** if seeking principal curvature coordinates on $\mathbf{p}$.

Equation (47) shows that there is a unique complex function of a complex variable, $w(\zeta)$, corresponding to any given minimal surface with principal curvature coordinates.

The lengths on the surfaces are given by L in **eq. (28)** in which

$$L^2 = \frac{1}{2}\left(\frac{d\mathbf{r}}{d\zeta}\right)\overline{\left(\frac{d\mathbf{r}}{d\zeta}\right)} = \frac{c^2\cosh^2 u}{2\left(\frac{dw}{d\zeta}\right)\overline{\left(\frac{dw}{d\zeta}\right)}}, \tag{48}$$

and $\overline{()}$ means the complex conjugate.

5 The Gauss map

The Gauss map is the image generated on a unit sphere by the unit normals to a surface. The coordinate curves $\theta^1 =$ constant and $\theta^2 =$ constant on the surface are mapped to corresponding curves on the sphere. The two surfaces $\mathbf{p}$ and $\mathbf{q}$ share the same normal and therefore they share the same Gauss map. The function $g(\zeta)$ in **sec. 3** is related to the Gauss map via the stereographic projection. If there are principle curvature coordinates on $\mathbf{p}$ and asymptotic coordinates on $\mathbf{q}$, then, upon differentiating **eq. (39)**,

$$\mathbf{n}_{,\alpha} = \frac{\left(-\sinh u\left(\cos v\,\hat{\mathbf{i}} + \sin v\,\hat{\mathbf{j}}\right) + \hat{\mathbf{k}}\right)u_{,\alpha} + \cosh u\left(-\sin v\,\hat{\mathbf{i}} + \cos v\,\hat{\mathbf{j}}\right)v_{,\alpha}}{\cosh^2 u}, \tag{49}$$

in which $\alpha = 1$ or 2. Thus

$$\mathbf{n}_{,1} + i\mathbf{n}_{,2} = \frac{\overline{\left(\frac{dw}{d\zeta}\right)}}{\cosh^2 u}\left(-\sinh w\,\hat{\mathbf{i}} + i\cosh w\,\hat{\mathbf{j}} + \hat{\mathbf{k}}\right). \tag{50}$$

Hence, upon comparing with **eq. (46)**,

$$\mathbf{n}_{,1} + i\mathbf{n}_{,2} = \frac{\left(\frac{dw}{d\zeta}\right)\overline{\left(\frac{dw}{d\zeta}\right)}}{c\cosh^2 u}\left(\mathbf{p}_{,1} - i\mathbf{p}_{,2}\right), \tag{51}$$

and

$$N^2 = \mathbf{n}_{,1}\cdot\mathbf{n}_{,1} = \mathbf{n}_{,2}\cdot\mathbf{n}_{,2} = \frac{\left(\frac{dw}{d\zeta}\right)\overline{\left(\frac{dw}{d\zeta}\right)}}{c\cosh^2 u} = \frac{c^2}{L^2}, \tag{52}$$
$$\mathbf{n}_{,1}\cdot\mathbf{n}_{,2} = 0.$$

Thus the side lengths, $N\delta\theta^\alpha$, on the curvilinear squares on the Gauss map are c divided by the side lengths on the minimal surfaces. If the coordinates are dimensionless, then c and L have the units of length and distances on the Gauss

map are dimensionless. The principal radii of curvature on $\mathbf{p}$ and $\mathbf{q}$ are equal to $\pm\rho$ where

$$\rho = \frac{L}{N} = \frac{L^2}{c} = \frac{c}{N^2}, \tag{53}$$

which is a special case of **eq. (15)**.

The minimal surfaces $\mathbf{p}$ and $\mathbf{q}$ can be constructed of unloaded fine grid cable nets in equilibrium with the cable tensions proportional to L to give a uniform surface tension. But the Gauss map can also be considered to be a grid structure in equilibrium, in which case the forces on each of its nodes from its members are the same as those on the nodes of the minimal surfaces $\mathbf{p}$ from its members. This is because the members on the two surfaces are parallel. But because of **eq. (51)** the tensions in one direction have to be replaced by compressions and *the magnitudes of these forces are now proportional to the reciprocal of the element lengths*.

Physically, an unloaded anticlastic surface in static equilibrium, which is a saddle-shaped surface with negative Gaussian curvature, must have both principal stresses in tension or both in compression. On the other hand, an unloaded synclastic surface with positive Gaussian curvature must have one tensile principal stress and one negative. This applies regardless of whether the directions of the principal stresses and principal curvatures coincide.

The equations of equilibrium (11.1.13) in Green and Zerna (1968, p. 387) reduce to

$$\begin{aligned} \nabla_\alpha \sigma^{\alpha\beta} &= 0, \\ a_{\alpha\beta}\sigma^{\alpha\beta} &= 0, \end{aligned} \tag{54}$$

for an unloaded sphere where $\sigma^{\alpha\beta}$ are the contravariant components of the membrane stress tensor, and $a_{\alpha\beta}$ are again the covariant components of the metric tensor. These equations are satisfied by

$$\sigma^{\alpha\beta} = \nabla^\alpha \phi \nabla^\beta \phi - \frac{1}{2} a^{\alpha\beta} \nabla^\lambda \phi \nabla_\lambda \phi, \tag{55}$$

subject to ϕ satisfying Laplace's equation,

$$\nabla_\alpha \nabla^\alpha \phi = 0, \tag{56}$$

which is consistent with the pattern of curvilinear squares that one associates with Laplace's equation. The gradient $\nabla\phi$ is in the direction of one or the other of the principal stresses.

However, if Laplace's **eq. (56)** applies to an entire sphere, the only possibility is that ϕ is constant, so there is no stress. Therefore, loads have to be applied to parts of the sphere, but the minimal surfaces $\mathbf{p}$ and $\mathbf{q}$ only correspond to the parts of the sphere which are unloaded. **Figure 1** shows the principal stress trajectories of a sphere loaded with equal and opposite wrenches, that is a combination of a force and a twisting moment, along the same axis. The axis is eccentric to the axis of the sphere.

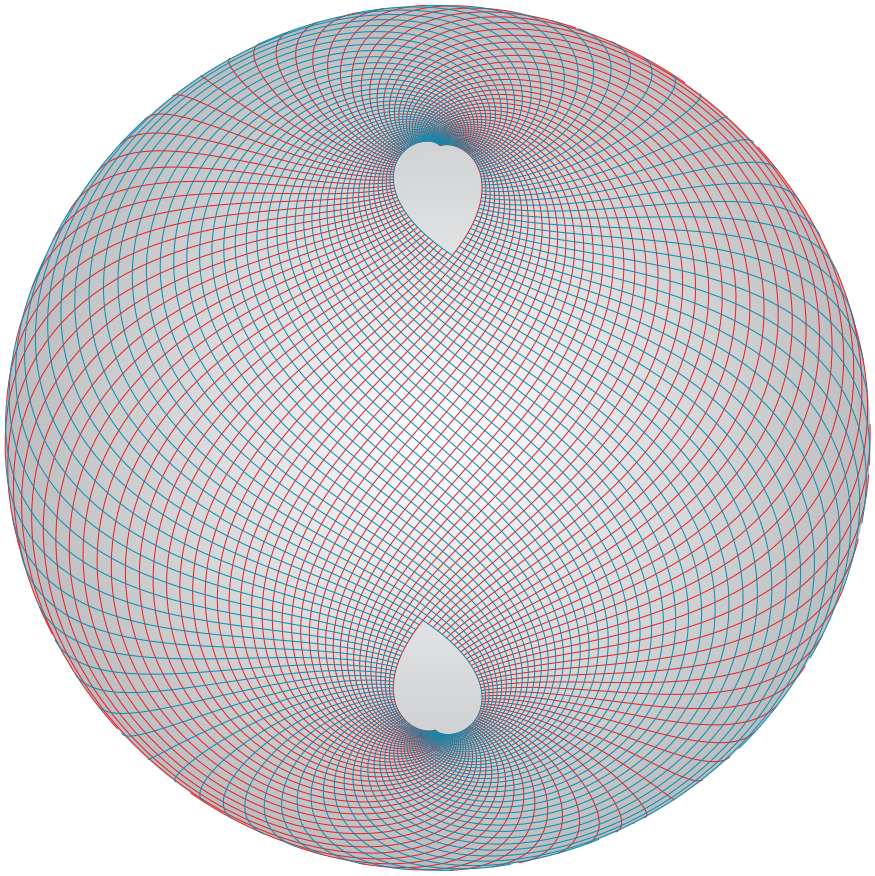

Figure 1: Sphere loaded with equal and opposite wrenches.

The pattern on the sphere is given by

$$e^w = \frac{\sinh \dfrac{\beta\zeta - \alpha}{2}}{\sinh \dfrac{\beta\zeta + \alpha}{2}}, \tag{57}$$

in which the surface coordinates are given by **eq. (18)** and the Cartesian coordinates on the sphere are given by **eq. (37)** and **(39)**. The real constant α controls the position of the wrenches and if $\alpha \to \infty$ the wrenches are applied at the north and south poles of the sphere. The complex constant β controls the ratio between the axial force and the twisting moment.

After some manipulation, the corresponding minimal surface is given by applying **eq. (47)** to produce

$$\mathbf{p} = \Re\left\{\frac{c}{\beta^2 \sinh\alpha}\begin{pmatrix}\cosh(\beta\zeta)\sinh\alpha\,\hat{\mathbf{i}}+\\ i\left(\sinh(\beta\zeta)\cosh\alpha-\beta\zeta\right)\hat{\mathbf{j}}+\\ \left(\sinh(\beta\zeta)-\beta\zeta\cosh\alpha\right)\hat{\mathbf{k}}\end{pmatrix}\right\}, \tag{58}$$

and a small part of the corresponding minimal surface is shown in **fig. 2**. If $\alpha \to \infty$ and $\beta = 1$ the minimal surface would be a catenoid and if $\alpha \to \infty$ and $\beta = (1+i)/\sqrt{2}$ the minimal surface would be a helicoid.

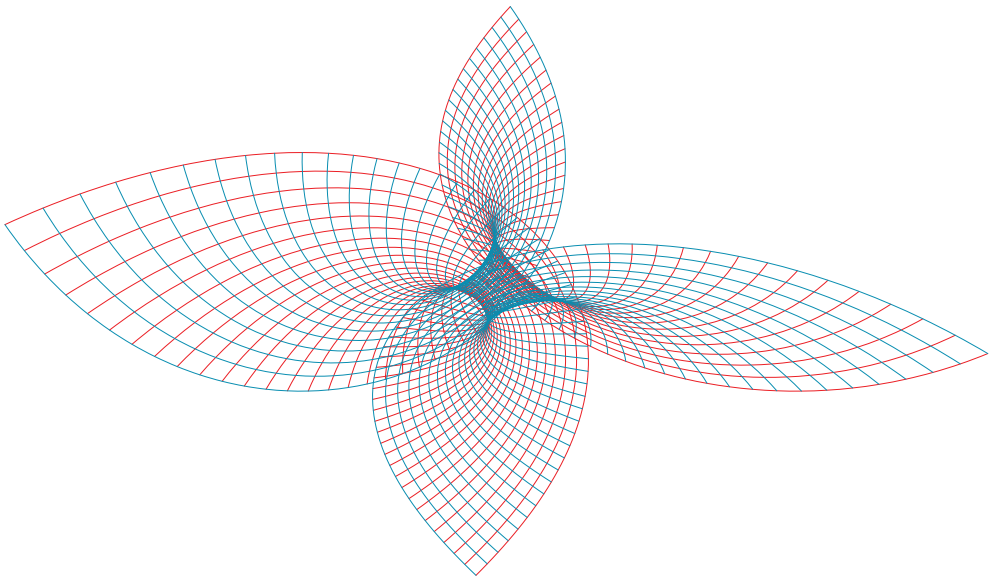

Figure 2: Minimal surface corresponding to small part of the Gauss map in **fig. 1**.

If $\beta = 1$ then there are equal and opposite axial forces, for any value of α. This corresponds to a source and a sink on the sphere, or on the stereographic projection of the sphere. If there is a source $X = A$ and sink at $X = 1/A$, where A is real, in the plane $Z = X + iY$ then one can write

$$\begin{aligned}\theta^1 + i\theta^2 &= \log\frac{(X+iY-A)}{\left(X+iY-\frac{1}{A}\right)},\\ \theta^1 &= \frac{1}{2}\log\left(\frac{X^2-2AX+A^2+Y^2}{X^2-2\frac{X}{A}+\frac{1}{A^2}+Y^2}\right),\\ \tan\theta^2 &= -\frac{Y\left(A-\frac{1}{A}\right)}{(X-A)\left(X-\frac{1}{A}\right)+Y^2},\end{aligned} \tag{59}$$

leading to the well known fact that the equipotential lines $\theta^1 =$ constant and $\theta^2 =$ constant from a source and sink are circles in the plane. These then map to circles on the sphere, which in turn means that the lines of principal curvature on the corresponding minimal surface lie in a plane (Abresch 1987; Tellier 2020).

6 Other unloaded pre-stressed grids in equilibrium with principal curvature cables or bars

Consider a pre-stressed surface structure $\mathbf{s}(\theta^1, \theta^2)$ in equilibrium with a fine grid of cables in tension or bars in compression which follow the principal curvature directions. Thus the cables or bars must be parallel to the corresponding lines on the Gauss map. The forces on the Gauss map will be equal or equal and opposite to those on in the pre-stress surface if the sphere is to be in equilibrium.

If the coordinate curves are in the principal curvature directions, then $\mathbf{s}_{,1}$ is parallel to $\mathbf{n}_{,1}$ and $\mathbf{s}_{,2}$ is parallel to $\mathbf{n}_{,2}$. Thus **eq. (51)** can be generalised to give

$$\begin{aligned} \mathbf{s}_{,1} &= \rho \mathbf{n}_{,1}, \\ \text{and} \quad \mathbf{s}_{,2} &= \chi \mathbf{n}_{,2}, \end{aligned} \tag{60}$$

where ρ and χ are the principal radii of curvature of $\mathbf{s}$. Hence

$$\mathbf{s}_{,12} = \rho_{,2}\mathbf{n}_{,1} + \rho \mathbf{n}_{,12} = \chi_{,1}\mathbf{n}_{,2} + \chi \mathbf{n}_{,12}. \tag{61}$$

Scalar multiplying by $\mathbf{n}_{,12}$ gives zero automatically and scalar multiplying by $\mathbf{n}_{,1}$ and by $\mathbf{n}_{,2}$ give

$$\begin{aligned} \rho_{,2} &= -(\rho - \chi)\frac{N_{,2}}{N}, \\ \text{and} \quad \chi_{,1} &= (\rho - \chi)\frac{N_{,1}}{N}, \end{aligned} \tag{62}$$

and hence

$$(\rho - \chi)(\rho + \chi)_{,12} - \rho_{,2}(\rho + \chi)_{,1} + \chi_{,1}(\rho + \chi)_{,2} = 0. \tag{63}$$

This is clearly satisfied by the sphere itself and by

$$\rho + \chi = \text{constant}, \tag{64}$$

which is a surface parallel to a minimal surface. It is also satisfied by a surface of revolution. **Equation (63)** means that such surfaces are related to Weingarten

surfaces, that is surfaces for which there is a functional relationship between the principal curvatures (Struik 1961).

7 Numerical form-finding of minimal surfaces

Adiels et al. (2018) describe form-finding techniques for a number of types of surface, but this paper is concerned with minimal surface. **Equation (24)**,

$$\mathbf{p}_{,11} + \mathbf{p}_{,22} = 0, \tag{65}$$

is satisfied by a fine grid cable net in which the force densities are constant. Such a net can easily be form found numerically by using matrix methods or dynamic relaxation (Barnes 1977).

In order to produce minimal surfaces, an isothermal grid needs to be imposed,

$$\begin{aligned} a_{11} = \mathbf{p}_{,1} \cdot \mathbf{p}_{,1} = a_{22} = \mathbf{p}_{,2} \cdot \mathbf{p}_{,2}, \\ \text{and} \quad a_{12} = \mathbf{p}_{,1} \cdot \mathbf{p}_{,2} = 0. \end{aligned} \tag{66}$$

Thus, using **eq. (65)**,

$$\begin{aligned} (a_{11} - a_{22})_{,11} + (a_{11} - a_{22})_{,22} = 0, \\ a_{12,11} + a_{12,22} = 0, \end{aligned} \tag{67}$$

which means that both $(a_{11} - a_{22})$ and a_{12} satisfy Laplace's equation. This means that if

$$\begin{aligned} a_{11} - a_{22} = 0, \\ \text{and} \qquad a_{12} = 0, \end{aligned} \tag{68}$$

are ensured at the boundary, then they will be zero everywhere (Williams 2011).

Note that the cables do not have to follow principal curvature directions and **eq. (68)** are sufficient.

If a soap film has a boundary which is a thread under tension, corresponding to a cable boundary for a real minimal surface tent, then equilibrium of the thread dictates that the curvature of the thread must be constant and lie in the local tangent plane to the soap film surface. This means that the boundary must be an asymptotic trajectory with constant geodesic curvature (Williams 2011). If this is the case, **eq. (68)** are particularly easy to apply and this was done to produce the cable nets in **fig. 3** in which the grid on the surface follows the asymptotic

directions for case (a) and principal curvature directions for case (b). The equations were solved using dynamic relaxation (Day 1965).

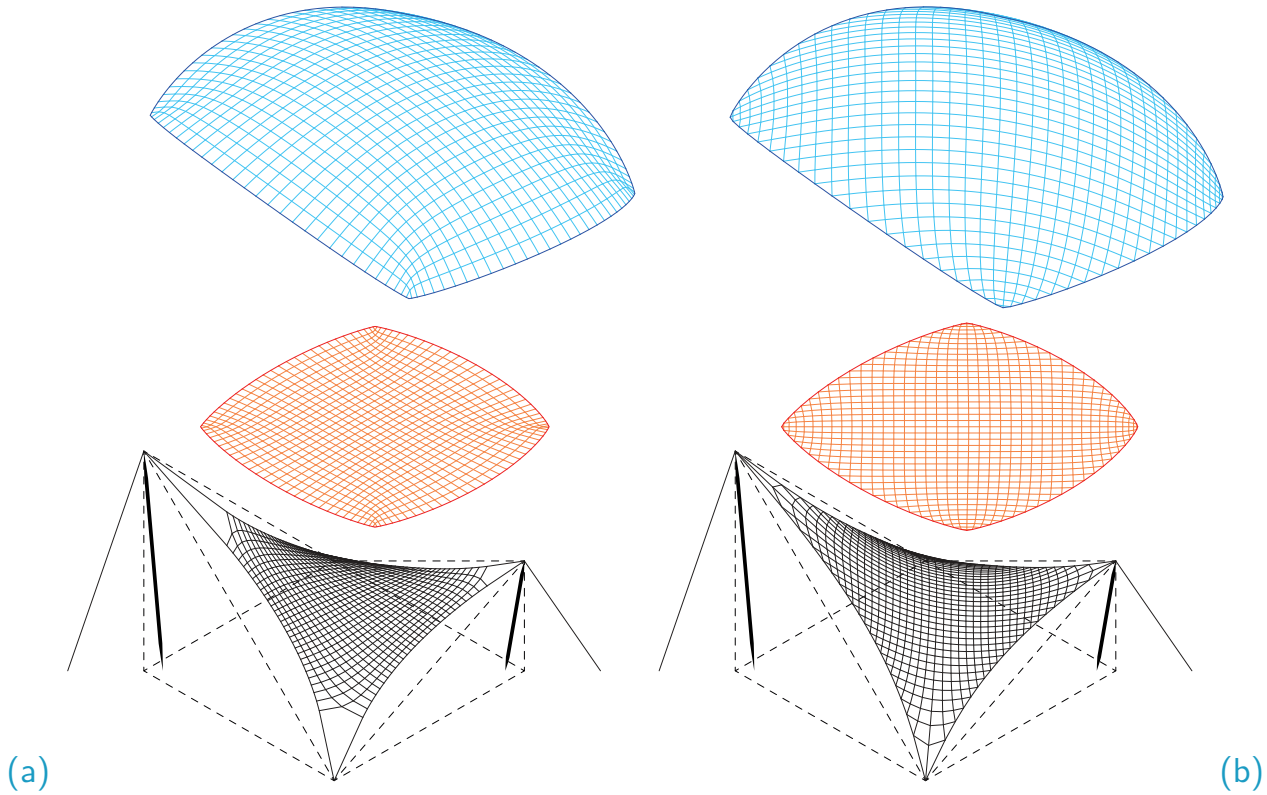

Figure 3: Numerically form found cable nets (bottom, black) with their Gauss map (top, blue) and the south pole stereographic projections of the Gauss maps (middle, red).(a) Asymptotic net and (b) Principal curvature net.

The members of the grid are given a constant force density, that is tension divided by length, and the nodes are allowed to slide along the boundaries to give a constant tension in the boundary cables. For the structures in **fig. 3** it was sufficient to just keep the boundary tension constant, but for **fig. 5** it was necessary to adjust the boundary tension according to the total length of the boundary for stability. This corresponds to the fact that the tension in a full circle boundary has to reduce if it gets smaller, so that a constant tension is unstable.

The asymptotic directions cross at right angles and therefore if the angle between two cables meeting at a support of the structure itself is less than 90°, then the curvature of the surface at the support is zero. This is the case for the cable nets in **fig. 3**, which can be seen clearly by visual inspection of the corners in the stereographic projection of the Gauss map where the node spacing tends to zero, corresponding to zero curvature. The asymptotic directions on the Gauss map are perpendicular to the directions on the structure itself and therefore the angle between the boundaries on the Gauss map is greater than 90° is it is less than 90° on the structure itself, and vice versa.

On the other hand, if the angle at the support is greater than 90°, then the *curvature of the surface at the support is infinite*. A soap film attached to a sphere will slide sideways until its tangent plane at the boundary to the sphere is normal to the sphere. This means that the boundary of the corresponding minimal surface will be a line of principal curvature with constant geodesic curvature. Such a boundary will be the three dimensional Cremona-Maxwell diagram (Rippmann 2016; Williams 1986) of a cable boundary and vice versa.

Frei Otto made soap film models as a starting point for several of his tensile structures, many with a loop of thread producing a hole in the surface (see the model photos in Vrachliotis et al. 2017, pp. 27, 43, 55) and **fig. 4** shows a physical model of such a 'Frei Otto eye' produced with a loop of wool. Before the loop is lifted out of the plane the loop is a pure circle. When it is first lifted there is an infinite curvature at the support until the angle reaches 90° when the curvature is finite. Further lifting produces zero curvature at the support.

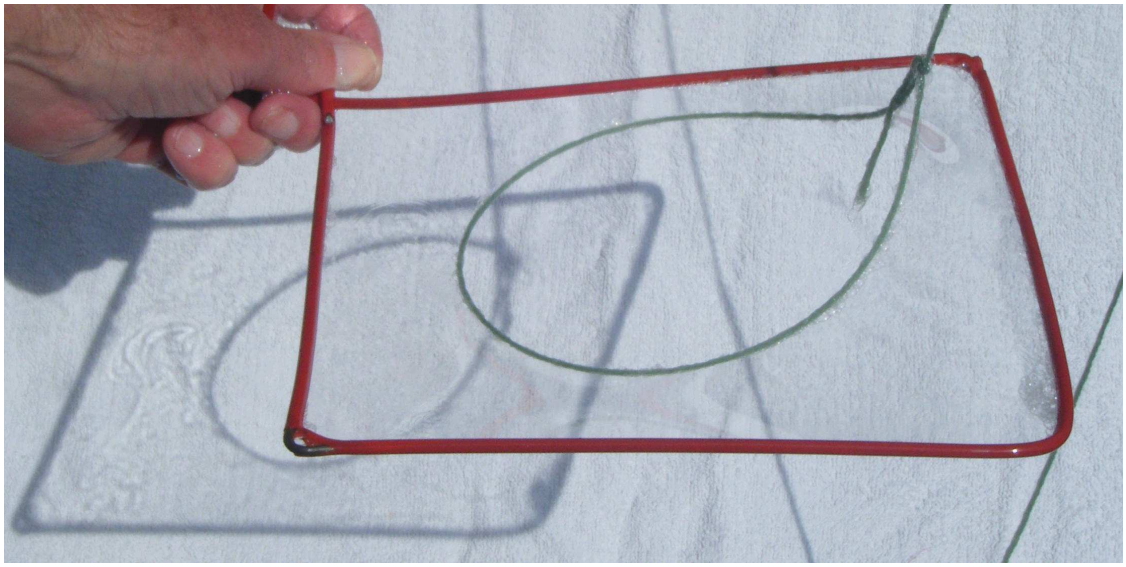

Figure 4: Physical model of Frei Otto eye.

Figure 5 shows a numerical simulation of the Frei Otto eye with a boundary approximating to a plane at infinity and lifted such that the angle at the support is 90° to give a finite non-zero curvature. The vertical force at the support can be calculated by considering the vertical force in the catenoid which the surface tends to at infinity. The black lines on the surface follow the asymptotic directions and form curvilinear squares.

Figure 6 is the stereographic projection of the corresponding Gauss map. **Figure 7** is an attempt at an analytical version of **fig. 6**. It begins with the map onto the complex plane of the stereographic projection,

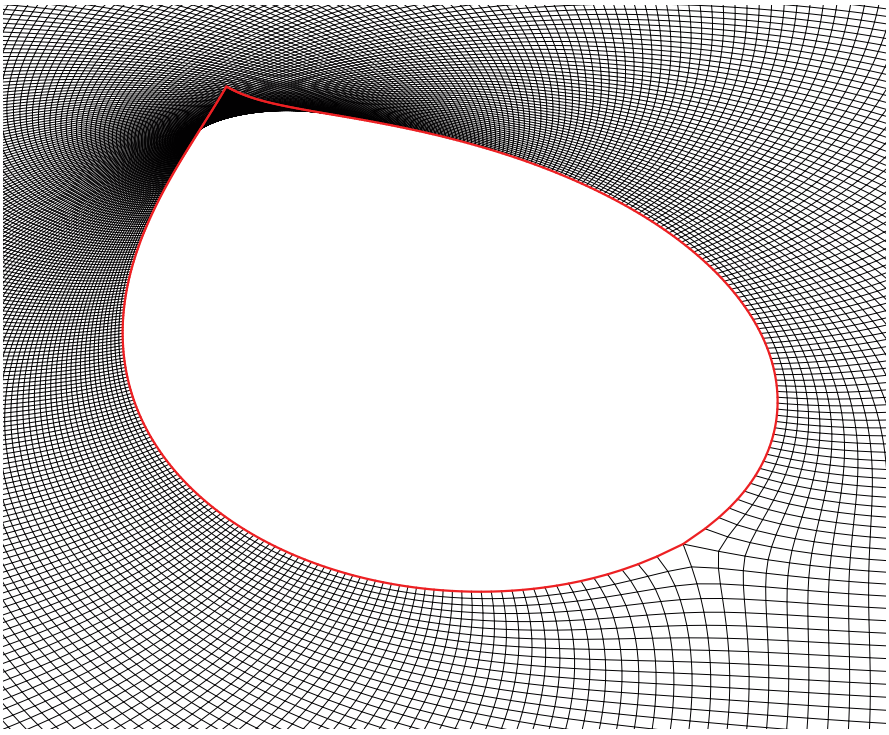

Figure 5: Numerical simulation of Frei Otto eye. The black lines on the surface follow the asymptotic directions and form curvilinear squares. The angle at the support is 90° to give a finite non-zero curvature.

$$Z = X + iY = e^w = \frac{(1+e^\pi)^{4/3} - 1}{(1+e^\eta)^{4/3} - 1}, \qquad \text{with} \quad \eta = \frac{(1+i)\,\zeta}{\sqrt{2}}. \tag{69}$$

The power of $4/3$ is there to produce the cusp which can be seen on the right hand side of **fig. 6** and **7**. The cusp corresponds to a position of zero curvature on the real surface, diametrically opposite to the support.

The formula in **eq. (69)** is augmented by adding a series of dipoles along the horizontal axis within the eye. A dipole is formed of a source and sink which are moved closer and closer together and increased in strength so that in the limit we have an infinitely strong source and sink infinitely close together. However, the resulting velocity is finite, except adjacent to the dipole. Future work will entail automatically modifying the strength of these dipoles so that the correct constant geodesic curvature is achieved on the boundary of the minimal surface. The geodesic curvature of the boundary on the real surface can be calculated from the stereographic projection directly. The reverse curvature direction in **fig. 6** and **7** arises from the stereographic projection rather than the Gauss map. The surface in **fig. 6** and **7** is outside the boundary, but if the north and south poles are swapped

in the stereographic projection, all the surface is within the boundary and infinity becomes a point. However if this is done it is very difficult to see the cusp.

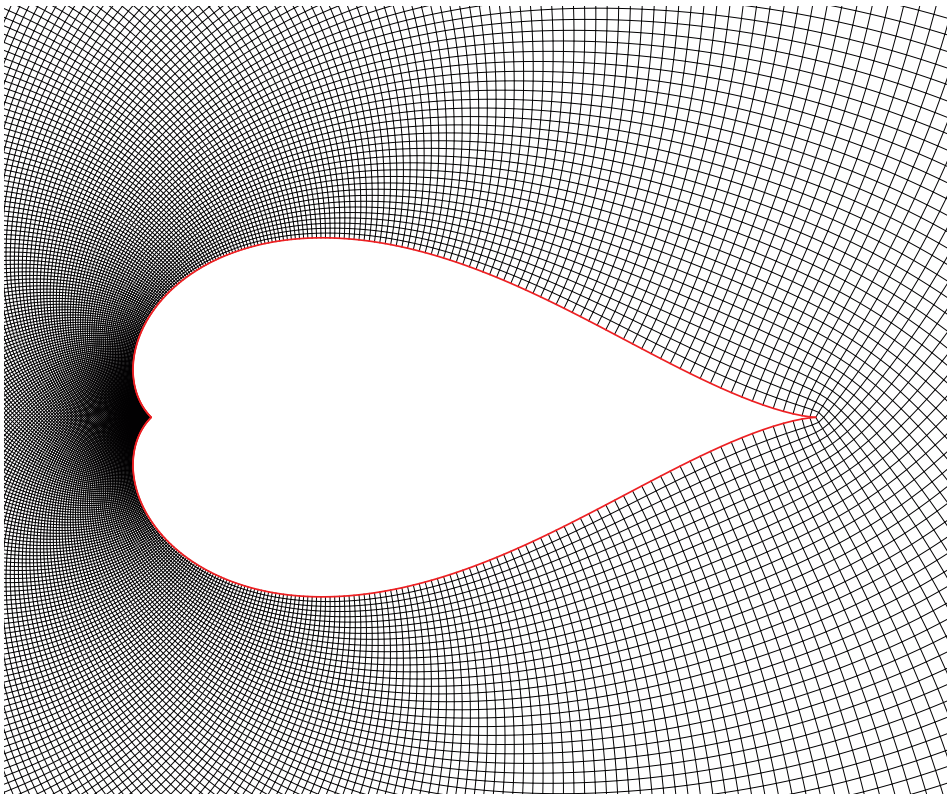

Figure 6: Stereographic projection of Gauss map of numerical simulation of Frei Otto eye.

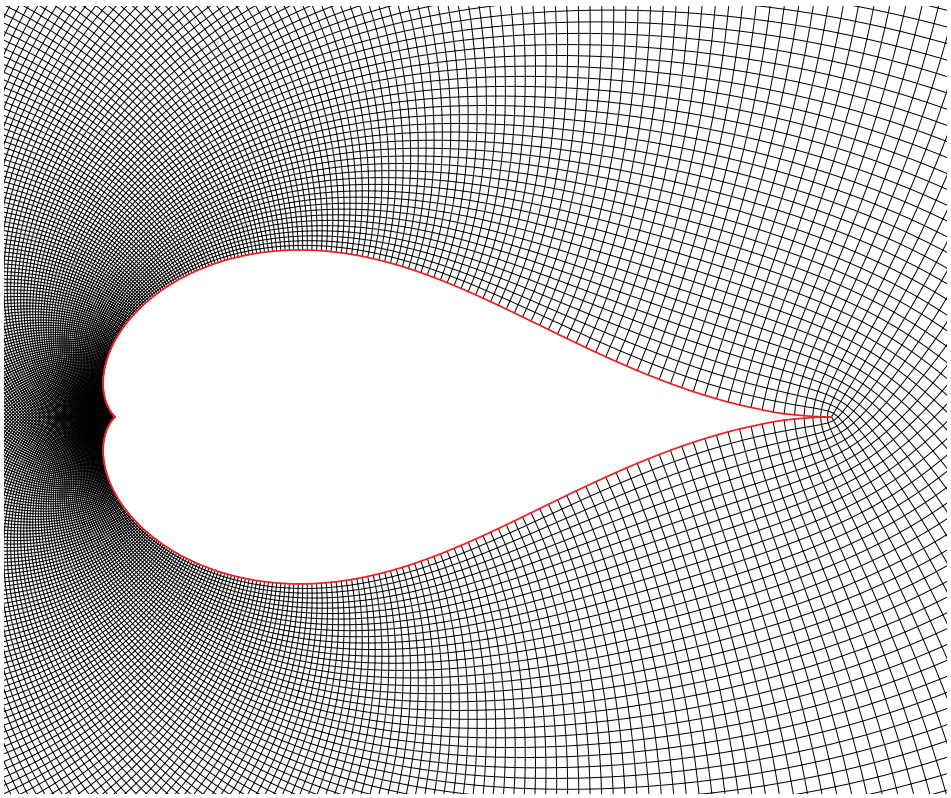

Figure 7: Analytic stereographic projection of Gauss map of Frei Otto eye.

8 Discussion

This paper has presented approaches that can be used to find minimal surfaces with principal curvature coordinate systems forming a grid of cables producing curvilinear squares on the surface in equilibrium under prestress but no load. The own weight and imposed loads would then be applied to the structure with the cables given the appropriate elastic stiffness.

It is shown how the Weierstrass–Enneper parametrisation can be constrained to map a set of complex points to a complex minimal surface where the real part has principal curvature coordinates and the imaginary part has asymptotic coordinates. The formulation is dependent on one complex analytic function which has to be integrated.

While analytical solutions are beautiful, the complexity of the technique may be overwhelming. Designing a cable net using the analytical approach requires skills in complex analysis and conformal mapping that most practising architects and engineers do not possess.

Alternatively numerical approaches may be used and it has been shown how to form find pre-stressed cable nets with cables following either principal curvature directions or asymptotic directions on the minimal surface. Proper implementation of such techniques, preferably using parallel computation for large cable nets, results in almost real time-response between input and output, just as for the analytical approaches.

References

Abresch, U. (1987, February). Constant mean curvature tori in terms of elliptic functions. *Journal für die reine und angewandte Mathematik (Crelles Journal) 1987*(374), 169–192.

Adiels, E., M. Ander, E. Hörteborn, J. Olsson, K.-G. Olsson, A. Sehlström, P. Shepherd, and C. Williams (2018). The use of virtual work for the formfinding of fabric, shell and gridshell structures. In L. Hesselgren, A. Kilian, S. Malek, K.-G. Olsson, O. Sorkine-Hornung, and C. Williams (Eds.), *Proceedings of the Advances in Architectural Geometry conference 2018*, pp. 286–315. Klein Publishing.

Arnold, R., C. Banister, A. Weir, D. Dabasia, and D. Goodliffe (2011, November). Delivering London 2012: the Velodrome. *Proceedings of the Institution of Civil Engineers - Civil Engineering 164*(6), 51–58.

Barnes, M. R. (1977). *Form finding and analysis of tension space structures by dynamic relaxation*. phdthesis, City University London.

Day, A. S. (1965). An introduction to dynamic relaxation. *The Engineer 219*, 218–221.

Dierkes, U., S. Hildebrandt, and F. Sauvigny (2010). *Minimal surfaces* (Second edition ed.), Volume 339 of *Grundlehren der mathematischen Wissenschaften*. Springer Berlin Heidelberg.

Douglas, J. (1931). Solution of the problem of Plateau. *Transactions of the American Mathematical Society 33*(1), 263–263.

Eisenhart, L. P. (1947). *An introduction to differential geometry, with use of the tensor calculus*. Princeton University Press.

Green, A. E. and W. Zerna (1968). *Theoretical elasticity* (2 ed.). Oxford University Press.

Harrison, J. and H. Pugh (2016). Plateau's problem. In J. F. Nash Jr. and M. T. Rassias (Eds.), *Open problems in mathematics*, Chapter 7, pp. 273–302. Springer International Publishing.

Hazewinkel, M. (1988). *Encyclopaedia of mathematics*. Springer Netherlands.

Krivoshapko, S. N. and V. N. Ivanov (2015). Weingarten surfaces. In *Encyclopedia of Analytical Surfaces*. Springer, Cham.

Nutbourne, A. W. (1986). A circle diagram for local differential geometry. In J. A. Gregory (Ed.), *The Mathematics of surfaces: The proceedings of a conference organized by the Institute of Mathematics and its Applications and held at the University of Manchester, 17-19 September 1984*, Oxford. Oxford University Press.

Otto, F. (1954). *Das hängende Dach: Gestalt und Struktur*. Bauwelt verlag.

Radó, T. (1933). *On the problem of Plateau*. Ergebnisse der Mathematik und ihrer Grenzgebiete. 2. Folge. Berlin: Springer-Verlag.

Rippmann, M. (2016). *Funicular shell design: geometric approaches to form finding and fabrication of discrete funicular structures*. Ph. D. thesis, ETH Zurich, Department of Architecture, Zurich.

Rogers, C. and W. K. Schief (2002, June). *Bäcklund and Darboux Transformations*. Cambridge University Press.

Schek, H.-J. (1974). The force density method for form finding and computation of general networks. *Computer Methods in Applied Mechanics and Engineering 3*(1), 115–134.

Shaeffer, R. (2013). History and development of fabric structures. In C. G. Huntington (Ed.), *Tensile fabric structures*, Chapter 1, pp. 1–24. American Society of Civil Engineers.

Spiegel, M. R. (1974). *Schaum's outline of theory and problems of complex variables with an introduction to conformal mapping and its application* (SI (matric) ed.). Schaum's outline series. McGraw-Hill Book Company.

Struik, D. J. (1961). *Lectures on classical differential geometry* (Second edition. ed.). Dover.

Tellier, X. (2020). *Morphogenesis of curved structural envelopes under fabrication constraints*. phdthesis, l'Université Paris-Est.

Tomlow, J. (2016). Designing and constructing the Olympic roof (Munich 1972). *International Journal of Space Structures 31*(1), 62–73.

Tsuboi, Y. and M. Kawaguchi (1966). The analysis and design of a suspension roof structure. In R. M. Davies (Ed.), *Space structures : a study of methods and developments in three-dimensional construction resulting from the International conference on space structures*, University of Surrey, pp. 925–945.

Vrachliotis, G., J. Kleinmanns, M. Kunz, and P. Kurz (2017). *Frei Otto: thinking by modeling* (1 ed.). Spector Books.

Weierstrass, K. (1866). Untersuchungen über die Flächen deren mittlere Krümmung überall gleich null ist. In *Math. Werke III*, pp. 612–625. Monatsber. Berliner Akad.

Wells, M. (2010). *Engineers: a history of engineering and structural design*. Routledge.

Williams, C. J. K. (1986). Defining and designing curved flexible tensile surface structures. In J. A. Gregory (Ed.), *The Mathematics of surfaces: The proceedings of a conference organized by the Institute of Mathematics and its Applications and held at the University of Manchester, 17-19 September 1984*, Oxford. Oxford University Press.

Williams, C. J. K. (2011). Patterns on a surface: the reconciliation of the circle and the square. *Nexus Network Journal 13*(2), 281–295.

Wise, C., A. Weir, G. Oates, and P. Winslow (2012). An amphitheatre for cycling: the design, analysis and construction of the London 2012 Velodrome. *The Structural Engineer 90*(6), 13–25.